Supplement of Geosci. Model Dev., 13, 4749–4771, 2020
https://doi.org/10.5194/gmd-13-4749-2020-supplement

Geoscientific Model Development
Open Access
EGU

Supplement of

Role of atmospheric horizontal resolution in simulating tropical and subtropical South American precipitation in HadGEM3-GC31

Paul-Arthur Monerie et al.

Correspondence to: Paul-Arthur Monerie (pmonerie@gmail.com)

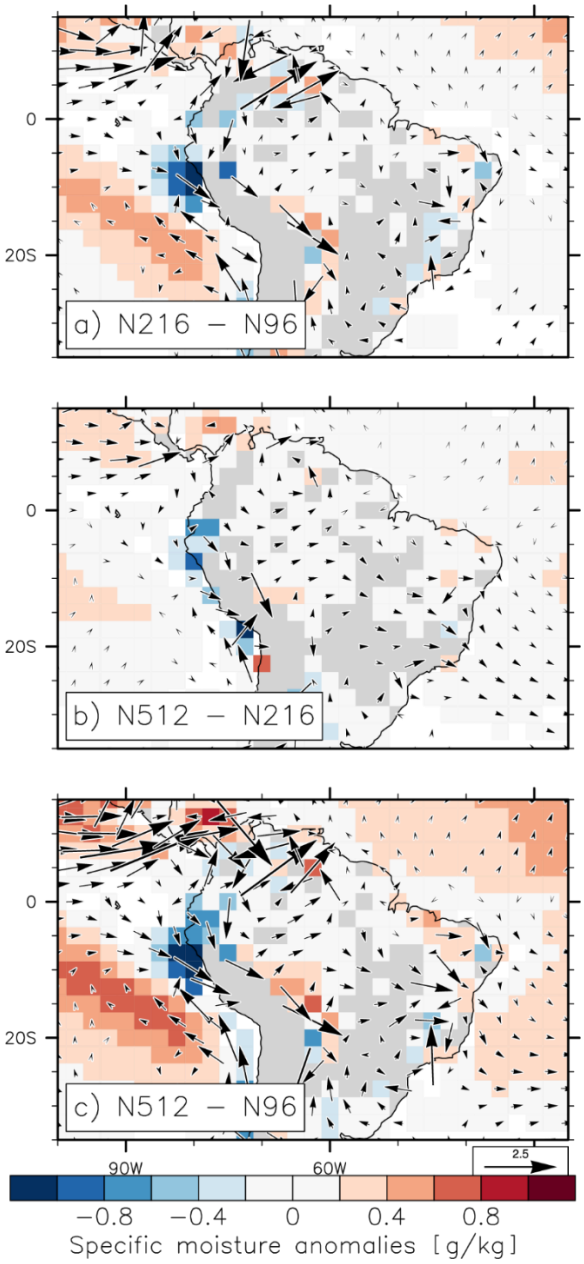

Figure S1: Ensemble-mean difference in annual mean surface specific humidity ($g.kg^{-1}$) and 850 hPa wind ($m.s^{-1}$), for (a) N216-N96, (b) N512-N216 and (c) N512-N96.

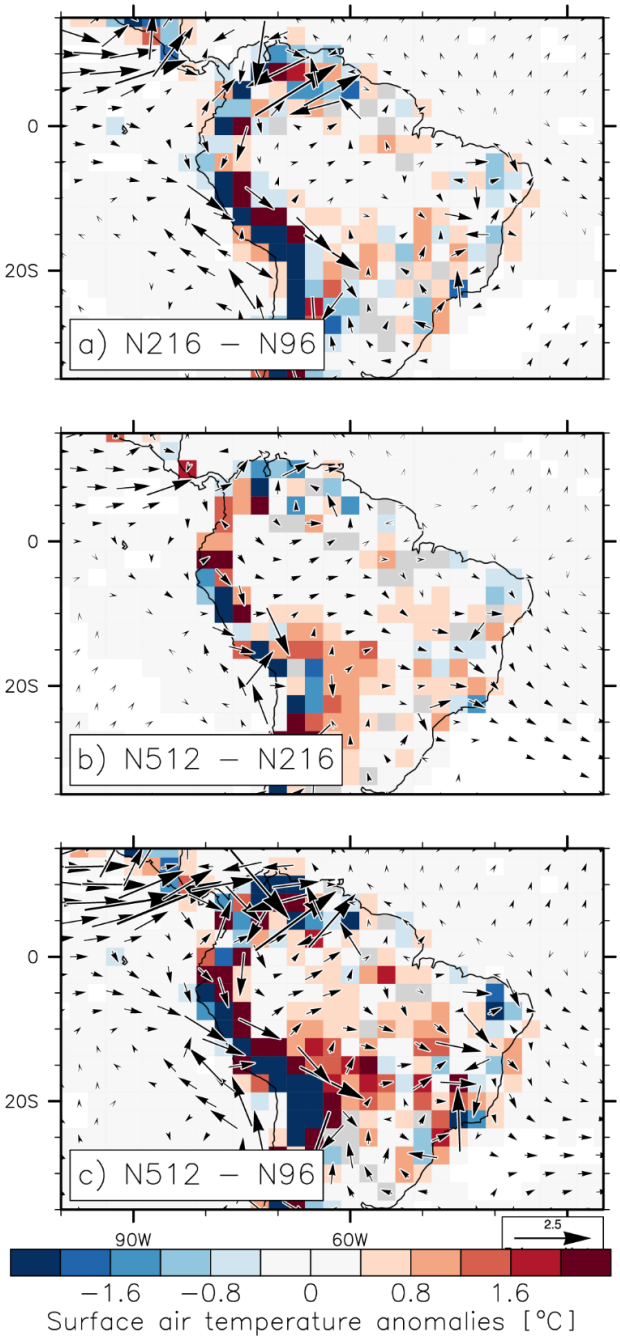

Figure S2: Ensemble-mean difference in annual mean surface air temperature (°C) and 850 hPa wind ($m.s^{-1}$), for (a) N216-N96, (b) N512-N216 and (c) N512-N96.

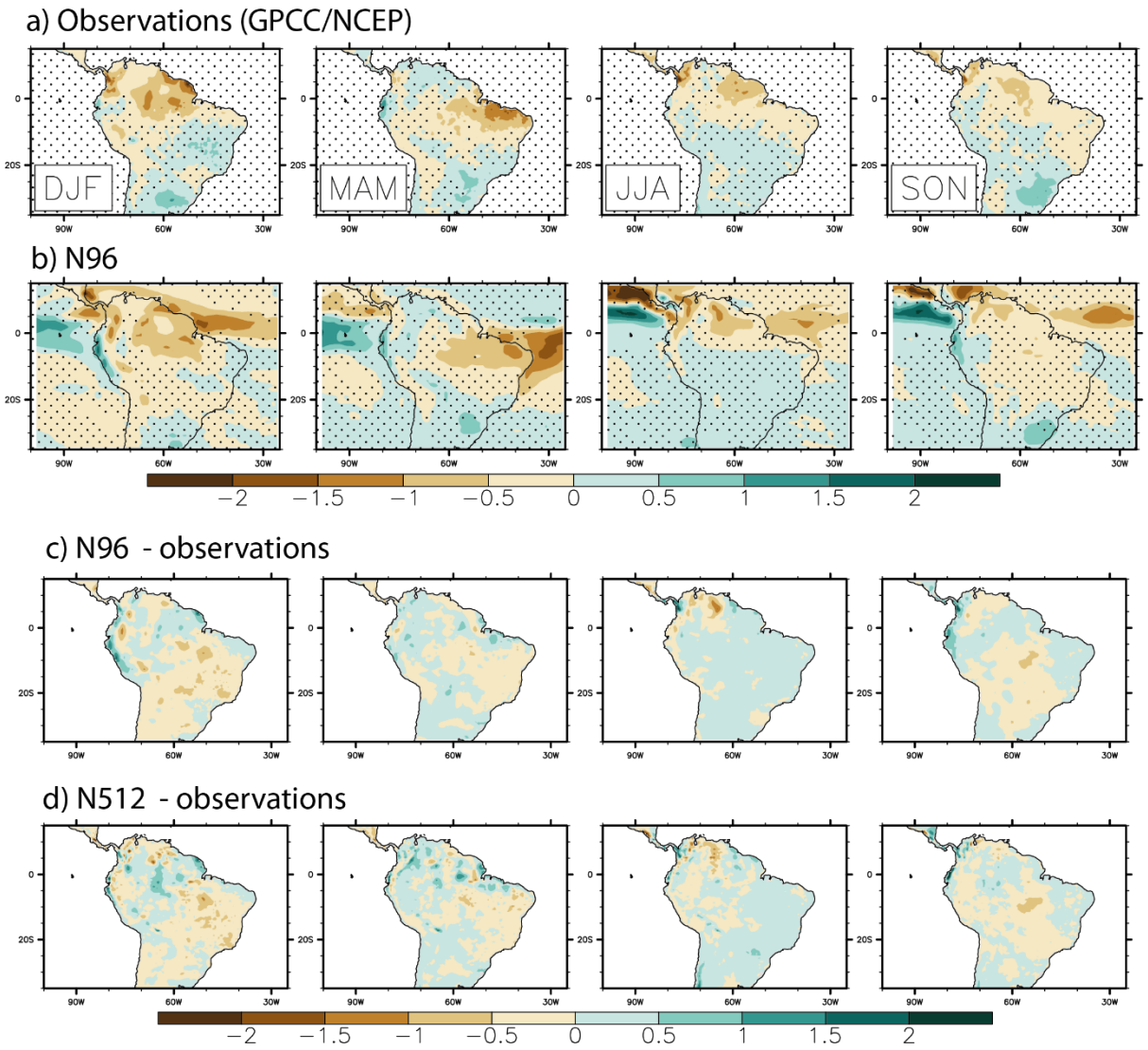

Figure S3: Precipitation regressed onto the EN3.4 index ($mm.day^{-1}.C^{-1}$) with (a) observations (GPCC for precipitation and NCEP for temperature), (b) N96. Stippling is added when regression is not significant, using a Student's t-test and a 95% confidence level. Difference between (c) N96 and observations (i.e. (b)-(a)) and (d) N512 and observations.

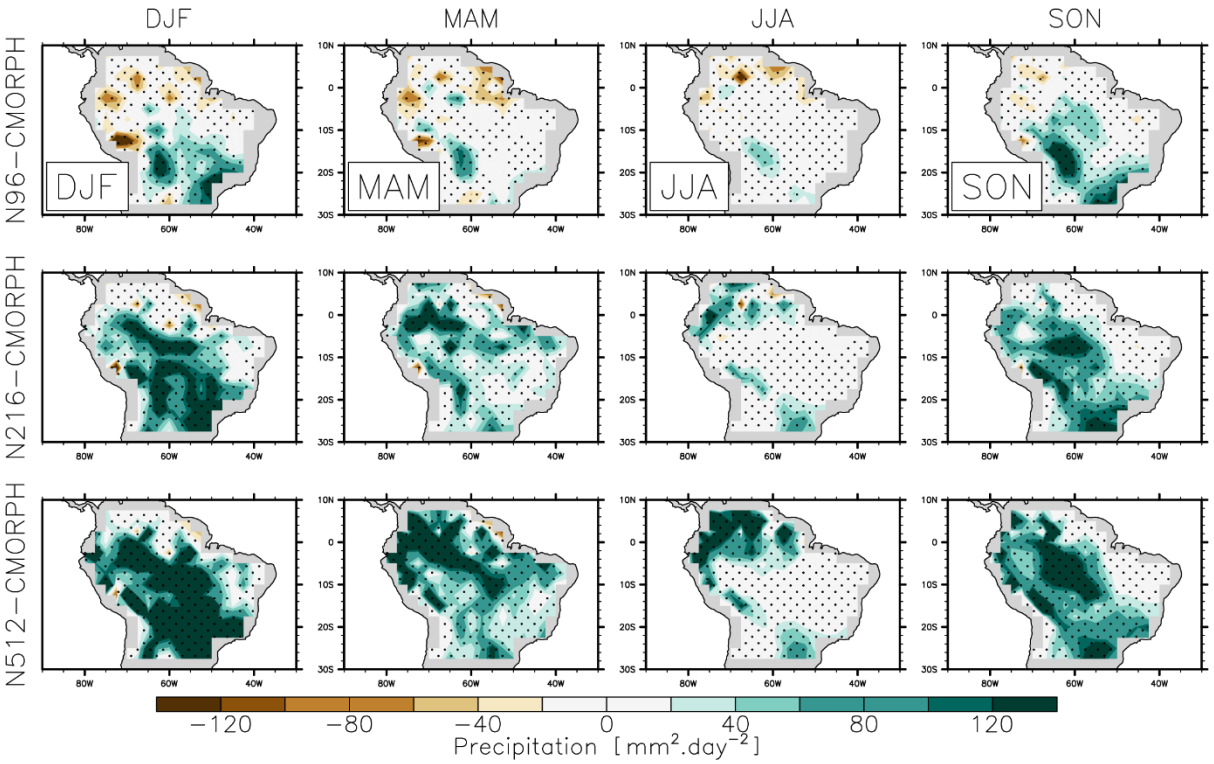

Figure S4: Bias in daily precipitation variance (mm^2.day-2) in (top row) N96, (middle row) N216 and (bottom row) N512, with regard to CMORPH. Results are given for the DJF, MAM, JJA and SON seasons, over the 1998-2014 period. Stippling indicates that differences are significant according to an f-test and a 95% confidence level.

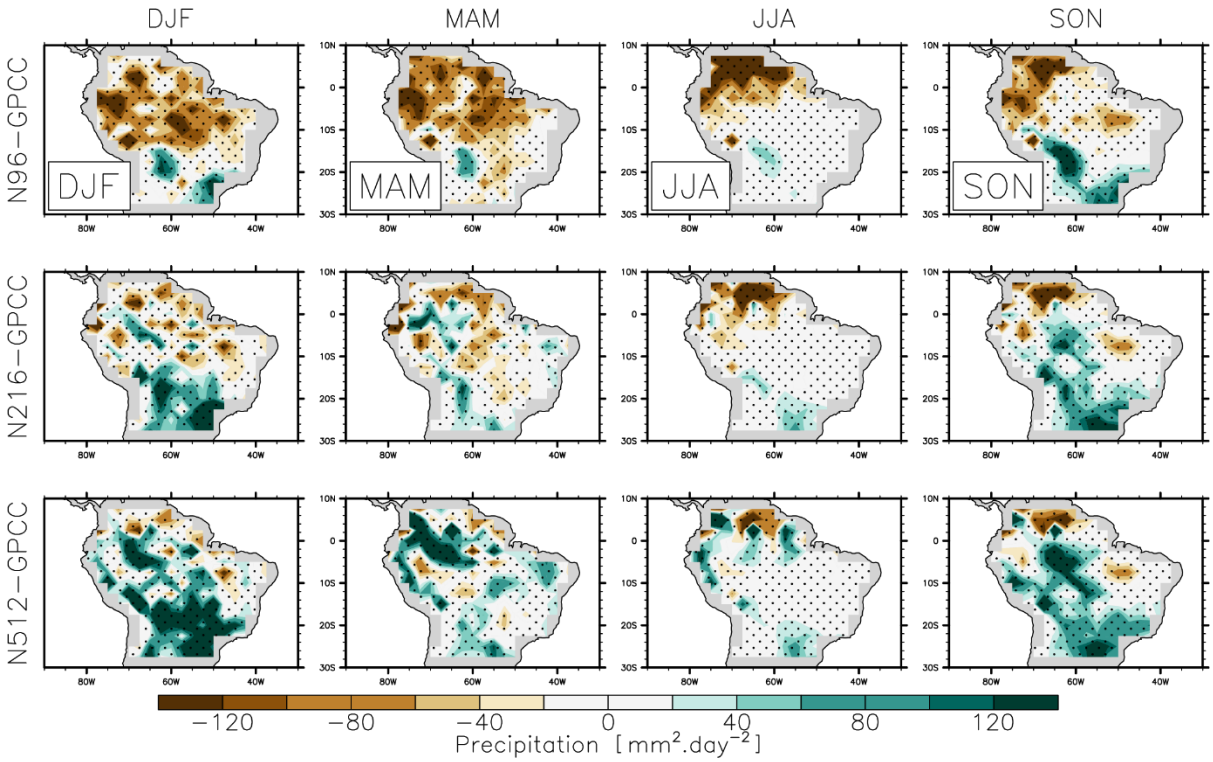

Figure S5: Bias in daily precipitation variance (mm^2.day-2) in (top row) N96, (middle row) N216 and (bottom row) N512, with regard to GPCC. Results are given for the DJF, MAM, JJA and SON seasons, over the 1998-2014 period. Stippling indicates that differences are significant according to an f-test and a 95% confidence level.

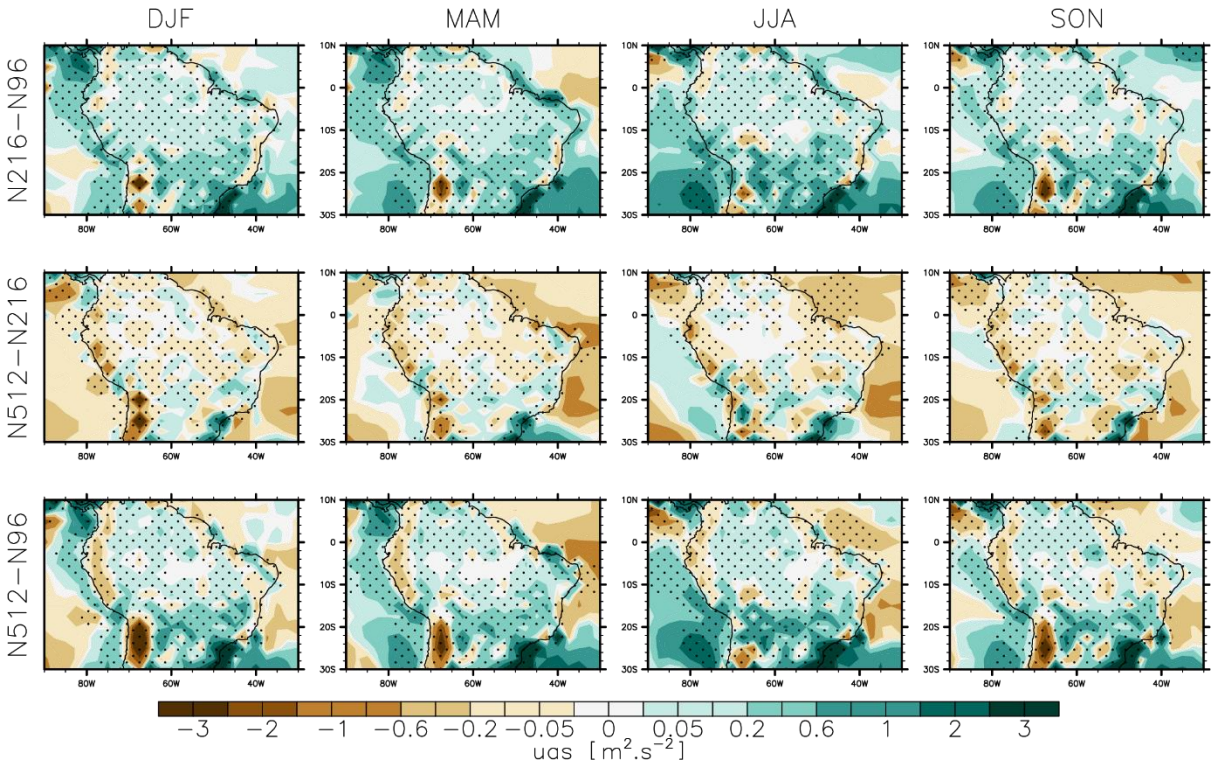

Figure S6: Ensemble-mean difference in surface zonal wind daily variance ($m^2.s^{-2}$), for (top row) N216-N96, (middle row) N512-N216 and (bottom row) N512-N96. Results are given for the DJF, MAM, JJA and SON seasons, over the 1998-2014 period. Stippling indicates that differences are significant according to an f-test and a 95% confidence level.

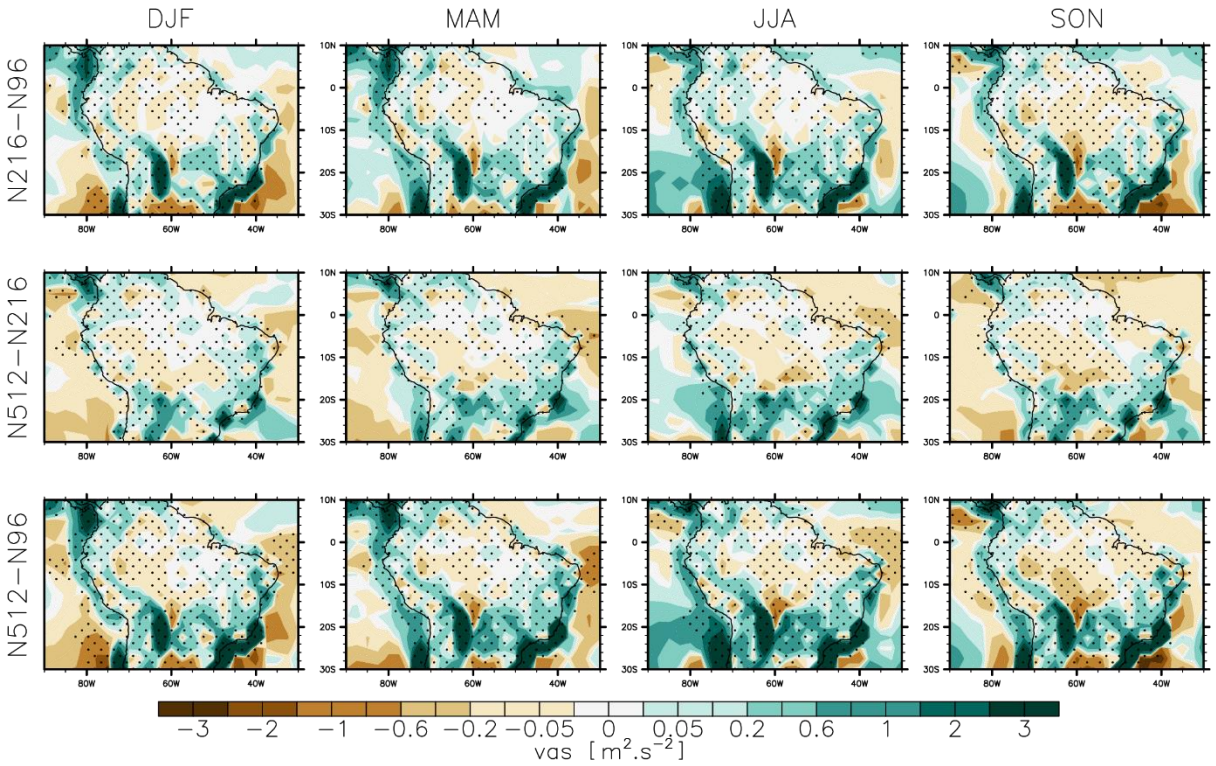

Figure S7: As in Figure S6 but for surface meridional wind.

.

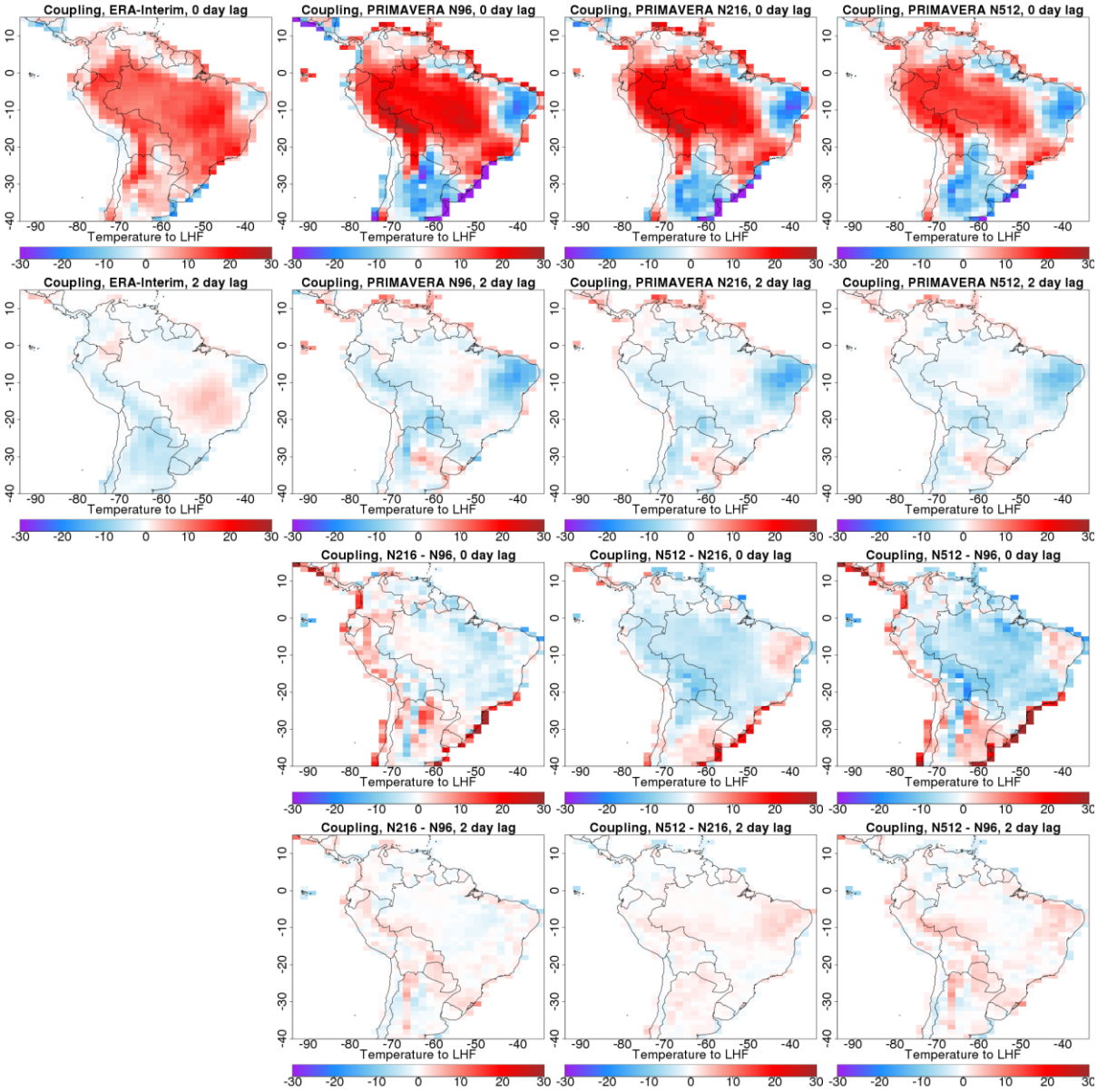

Figure S8: Coupling strength ($r_{a,b}\sigma_b$) between daily temperature and latent heat flux during the southern summer wet season (DJF). Daily data from PRIMAVERA model ensembles (1950-2014) at 3 resolutions, and ERA-Interim reanalysis (1979-2014). Showing the results from ERA-Interim, differences between PRIMAVERA and ERA-Interim results, and differences between PRIMAVERA results at different resolutions, for 0 time lags and 2 day time lags (the soil situation 2 days after precipitation).

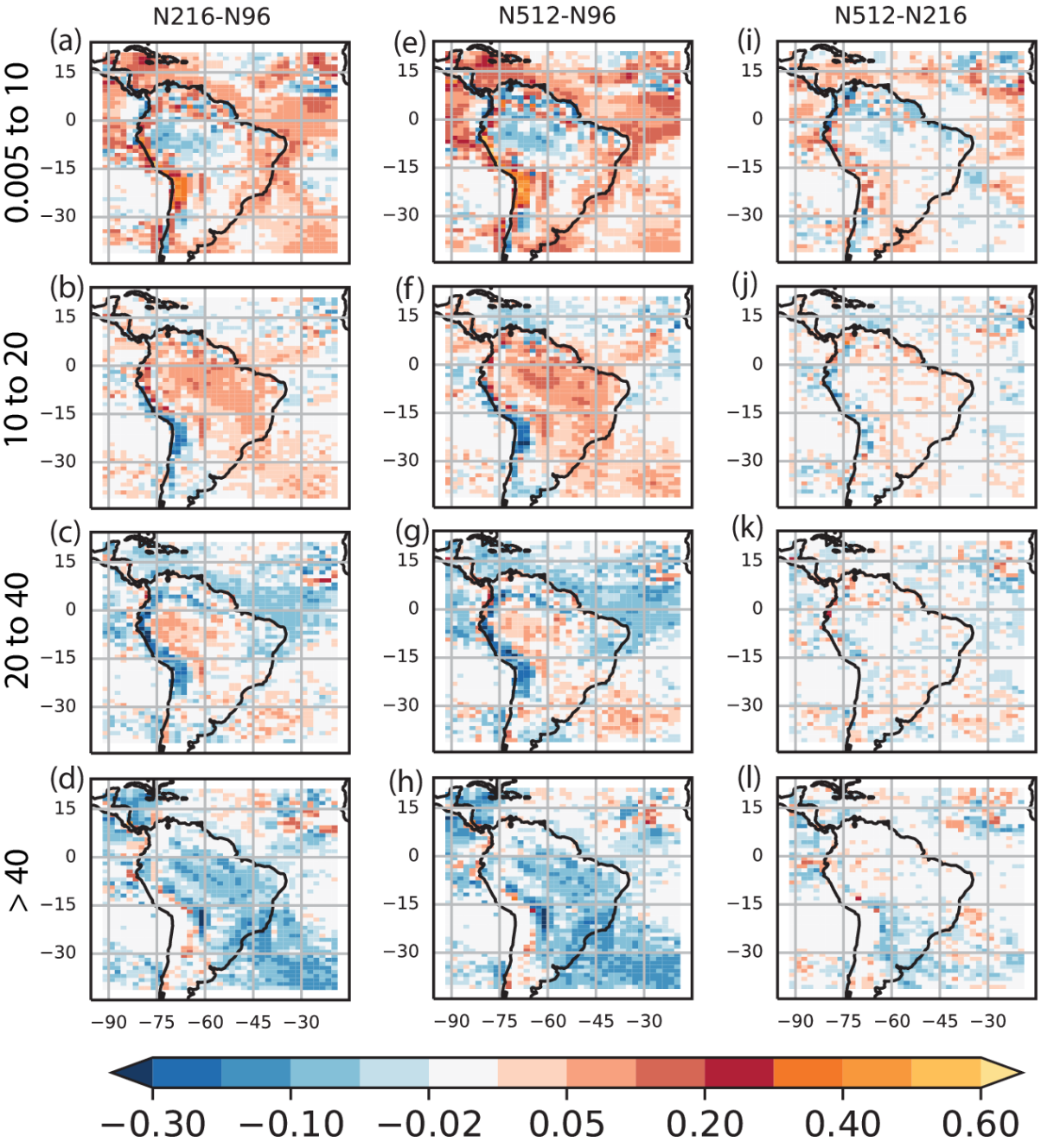

Figure S9: Differences in the fractional contribution to the total precipitation rate from ranges of intensity bins shown in the labels above each pane between N216 and N96 (a-d). The four ranges of intensity bins are (a) 0.005 to 10 mm/day, (b) 10 to 20 mm/day, (c) 20 to 40 mm/day and (d) >40 mm/day. Same as for N96-CMORPH but for N512 and N96 (e-h) and N512 and N216 (i-l).

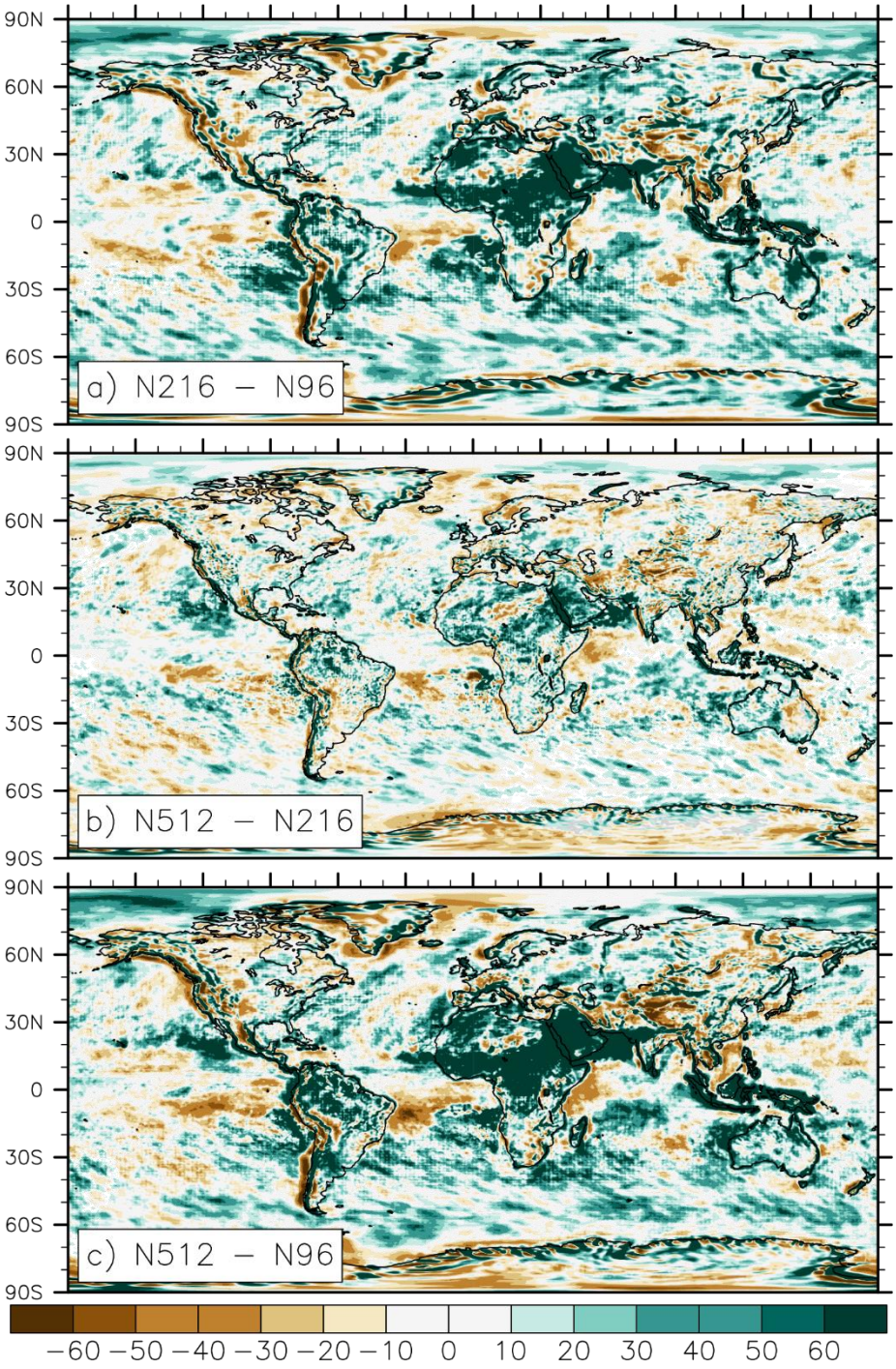

Figure S10: Ensemble-mean difference in annual mean precipitation variance (in %) for (a) N216-N96, (b) N512-N216 and (c) N512-N96.